Matching Image Objects in Dynamic Pedobarography

João Manuel R. S. Tavares, J. Barbosa, A. Jorge Padilha

FEUP - Faculdade de Engenharia da Universidade do Porto
INEB - Instituto de Engenharia Biomédica
Praça Coronel Pacheco, nº 1
4050–453 PORTO
emai: {tavares, jbarbosa, padilha}@fe.up.pt

Abstract: *The paper presents an approach for matching image objects in dynamic pedobarography image sequences, based on finite element modelling of the objects and on modal analysis of the of the object models.*
The proposed approach allows the determination of correspondences between two distinct images, using either 2D or 3D modelling. The displacement vectors for the nodes of the matched object models are also determined, based on which the deformation energy is computed.
The deformation energy can be used as a global measure of the similarity of the matched objects.

Keywords: *Computer vision, computer graphics, finite element models, modal analysis, deformable models, dynamic pedobarography.*

1. INTRODUCTION

One of the main problems in computer vision consists in the determination of object correspondences in different images and on the computation of robust canonical descriptors used for the recognition of 2D and 3D objects, either rigid or non-rigid.

In this paper a methodology to address the above problem is presented, adapting the approach initially proposed by Sclaroff [1, 2], and results of its application to the analysis of dynamic pedobarography image sequences are discussed.

Figure 1 displays a diagram of the proposed method. The locations of the image data points $X = [X_1 \cdots X_m]$ in each image are used as the nodes for building a finite element model[1] of elastic material. Next, the eigenmodes $\{\phi\}_i$ of the model are computed, providing an orthogonal description of the object and its natural deformations, ordered by frequency. The eigenvectors, also called shape vectors for each mode [4, 5], describe how each mode deforms the object by changing the original data point locations: $X_{\text{deformed}} = X + a\{\phi\}_i$.

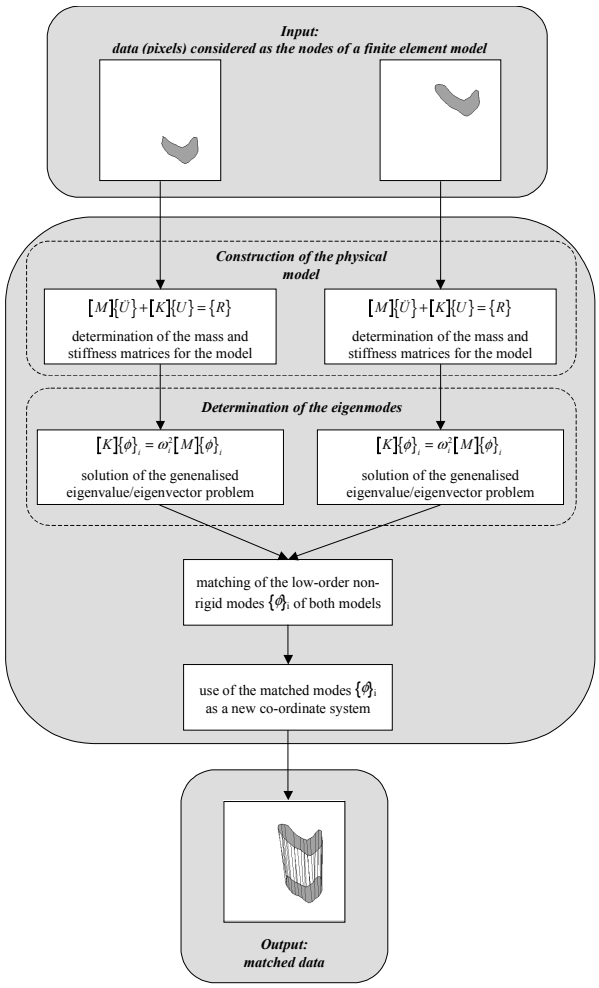

Figure 1. Diagram of the methodology.

The first three (in 2-D) or six (in 3-D) modes are the rigid body modes of translation and rotation; the remaining modes are non-rigid [4, 5]. In general, lower frequency modes describe global deformations while higher frequency modes essentially describe local deformations. This type of ordering from global to local behaviour is quite useful for object pairing and comparison.

The eigenmodes also form an orthogonal, object-centred

[1] Since the first use in computer vision of the finite element method, by Pentland in 1989 [3], it has expanded into many areas, such as rigid and non-rigid motion analysis, face recognition, image representation, image matching and object description.

co-ordinate system for the location of the point data, that is, the location of each point is uniquely described, in terms of the displacement for each eigenmode. The transformation between the Cartesian image co-ordinates and the modal system co-ordinates is achieved through the eigenvectors of the finite element model.

Two groups of image data points, corresponding to two different images in a sequence, are to be compared in the modal eigenspace. The main idea is that the low order modes of two similar objects will be very close even in the presence of affine transformation, non-rigid deformation, local shape variation, or noise.

Using the above concept data correspondence is determined by modal matching. This process obtains a number of highly reliable data point matches; the displacement of other points will then be estimated by using the physical model as a smoothing restriction, in a manner similar to the one used for active contour models [1, 6].

Finally, based on the correspondence of many of the data points of the two objects, their shape differences can be measured. As the modal analysis decomposes the deformation in an orthogonal set, one can selectively measure rigid body differences, low-order projective variations, or essentially local deformations. The process is quite flexible and general.

Alternatively, one can align two objects or distort one object's shape to fit the shape of the other. This alignment and distortion process is useful in fusing data obtained from different sensors or in registering image data acquired under different conditions. It is also useful in computer graphics applications, where the process is known as morphing.

The modal representation is supported by biologists involved in studying the morphology of animal skeletons and shapes, according to which the shapes of different species are related by deformation [1]. Recent studies also use modal deformation analysis to describe the growth of animal organs and to match organs of the same type [7, 8, 9].

In short, the modal analysis technique offers three advantages over other methods: i) it can automatically identify and label corresponding points in two objects, allowing for their registration, comparison and morphing; ii) the modal representation separates different types of deformation; iii) the deformation parameters correspond qualitatively to what is believed to be also used by humans and thus they can be used for animation and database searching [1].

One possible disadvantage of the method is the computational cost for determining the eigenmodes, which can be very high when the number of object data points is very large. This problem can be addressed by using multi-resolution models [1, 2]. Moreover, for particular classes of similar objects the modes can be predetermined and generalised [10], and in some cases, for tubular and spherical topologies, Nastar ([11]) demonstrates that the eigenmodes can be obtained analytically.

The following sections present a brief introduction to dynamic pedobarography, the object models used and some experimental results. Final conclusions are drawn and further work is identified.

2. DYNAMIC PEDOBAROGRAPHY

Pedobarography refers to measuring and visualising the distribution of pressure under the foot sole. The recording of pedobarographic data along the duration of a step in normal walking conditions permits the dynamic analysis of the foot behaviour; the introduction of the time dimension augments the potential of this type of clinical examination as an auxiliary tool for diagnostics and therapy planning [12].

The basic pedobarography system consists of glass or acrylic plate trans-illuminated through its polished borders in such a way that the light is internally reflected; the plate is covered on its top by a single or dual thin layer of soft porous plastic material where the pressure is applied (see Figure 2).

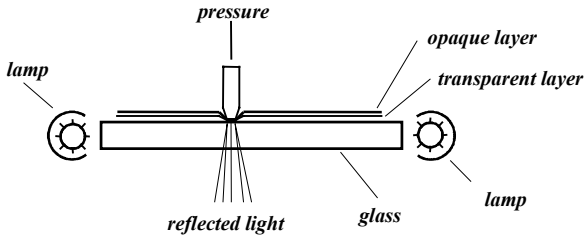

Figure 2. Basic (pedo)barography principle.

When observed from below, in the absence of applied pressure, the plate is dark; when pressure is applied on top of the plastic layer, the plate displays bright areas that correspond to the light crossing the plate after reflection on the plastic layer; this reflection occurs due to the alteration of the local relation of light refraction indices resulting from the depletion of the air interface between the glass plate and the plastic layer. A good choice of materials and an adequate calibration of the image acquisition system allow a nearly proportional relation between the local pressure and the observed brightness.

Using a practical set-up as the one shown in Figure 3, a time sequence of pressure images is captured; Figures 4-9 show a few of the images captured in a sample sequence (displayed with inverted brightness); the image data is very dense, as opposed to other measuring methods, and very rich in terms of the information it conveys on the interaction between the foot sole and the flat plate.

3. OBJECT MODELS

In the initial stages of the work, the object contours in each image were extracted and the matching process was oriented to the contours' pixels. A practical difficulty arising from this approach is the possible

existence of more than one contour for the object in each image; two possible solutions were considered, upon labelling the various contours in each image: i) use of a Kalman filtering[2] approach to estimate and track the location of the contours' centroids in the image sequence; ii) use of a measure of the deformation energy to align two contours, selecting the lower energy pairs.

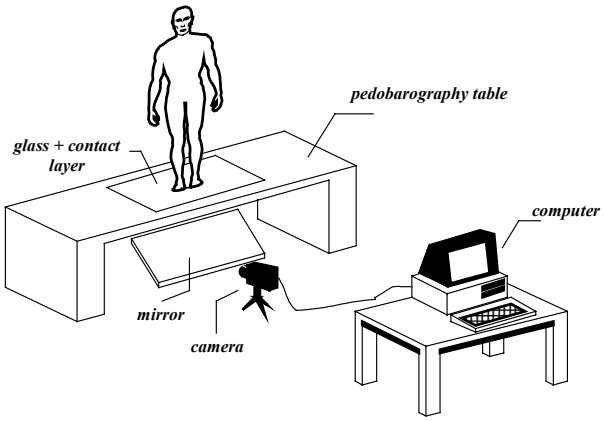

Figure 3. Set-up of a pedobarography system.

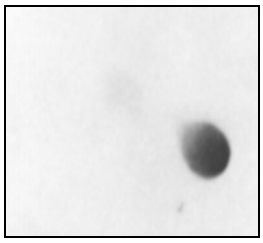

Figure 4. Image 4 of a sample sequence.

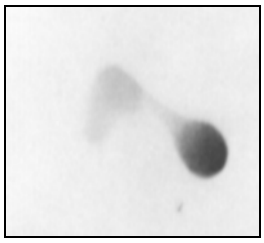

Figure 5. Image 5 of a sample sequence.

Figure 6. Image 6 of a sample sequence.

Figure 7. Image 7 of a sample sequence.

Figure 8. Image 8 of a sample sequence.

Figure 9. Image 9 of a sample sequence.

However, an additional problem is present: the possibility that along the image sequence various contours will merge or split. In order to accommodate this possibility a new model has been developed, similar to the one used in various applications with controlled environment, such as in face analysis and recognition [14, 15, 16, 17]. The brightness level of each pixel is considered as the third co-ordinate of a 3-D surface point. The resulting single surface model solves the two aforementioned problems.

The use of the surface model also simplifies the consideration of isobaric contours, which are important in pedobarographic analysis, either for matching contours of equal pressure along the time sequence or for matching contours of different pressure in a single image.

The following sections describe the object models used and their construction. Each model has its own advantages and shortcomings; for every particular problem, the best choice must be made.

3.1. Contour Model

Two modelling approaches were used to determine the correspondence and the deformation energy among two contours in distinct images:

- A single 2D isoparametric Sclaroff model is used for each contour. In building this type of element no previous ordering of the nodes is required; Gaussian shape functions are used. The method to determine the mass and stiffness matrices for this 2D element is described in e.g. [1, 2].
- Each contour is built by linear axial 2D finite elements (Figure 10). For this type of discretisation a previous ordering of the contour nodes is required. The matrix formulation for these elements can be found in [5], for example.

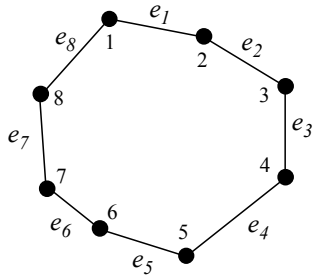

Figure 10. Modelling of a contour by a set e_i of axial finite elements.

Standard image processing and analysis techniques are used to determine the contour pixels, namely thresholding, edge enhancement, hysteresis line detection and tracking [13]. For example, Figures 12 and 13 show an intermediate result and the final contour determination for the image in Figure 11.

[2] See [13], for example.

Figure 11. Image (negated) where contours must be found.

Figure 12. Result image after edge enhancement.

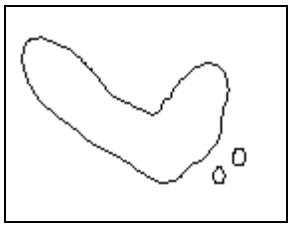

Figure 13. Contours obtained by a line detection and tracking algorithm with hysteresis.

3.2. Surface Model

For the surface model, two approaches were also used:

- A single 3D isoparametric Sclaroff finite element model is used for each surface. Again it must be noticed that there is no requirement for previous ordering of the nodes. The matrix building for these finite elements can be found in [1].
- Each surface is built by linear axial 3D finite elements (Figure 14). The previous ordering of the surface nodes is required. The matrix formulation for these finite elements can be found in [5], for example.

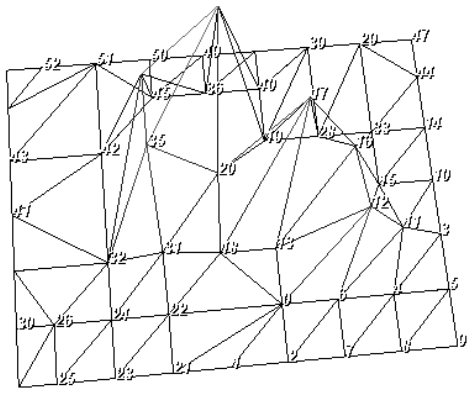

Figure 14. Modelling of a surface by a set of axial 3D finite elements. Each node is connected to its neighbours through axial elements.

The method to determine the nodes that form the surface in each image can be summarised as follows:

1. noise pixels (that is, pixels with brightness lower than a calibration threshold) are removed and a Gaussian-shaped smoothing filter is applied to the image (Figure 15);
2. the circumscribing rectangle of the object to be modelled is determined and the image is sampled within that area (Figure 16);
3. a 2D Delaunay triangulation[3] is performed on the sampled points, using the point brightness as the third co-ordinate;
4. the triangular mesh is simplified using a decimation algorithm[3] in order to reduce the number of nodes and thus the computational cost;
5. a Laplacian smoothing algorithm[3] is used to reduce the high frequency noise associated to the mesh;
6. a scale change is performed on the third co-ordinate (derived from brightness) in order to have similar ranges of values in all co-ordinates (Figure 17).

Figure 15. Image (negated) after noise removal and Gaussian filtering.

Figure 16. Object sampling.

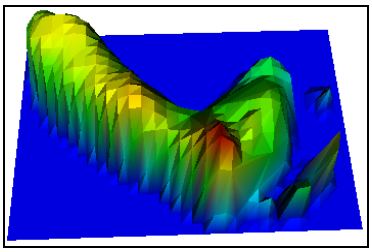

Figure 17. Resulting surface.

3.3. Isobaric Contour Model

As in the two previous models, the approaches used to match isobaric contours and to determine the deformation energy are:

- A single Sclaroff isoparametric finite element, either 2D or 3D, to model each contour.
- Linear axial finite elements, either 2D or 3D, to build the contours.

The isobaric contours are extracted (Figure 18) after using the procedure described in the previous section.

4. Experimental Results

The methodology just presented has been implemented in *Microsoft Visual C++*, for *Microsoft Windows 95/98/NT* platforms; the system also integrated the *C++ Newmat* [20] library for matrix computation and the *C++ VTK - The Visualization Toolkit* - [18, 19] for 3D

[3] See, for example, [18, 19].

visualisation, for mesh triangulation, simplification and smoothing, and for the extraction of isobaric contours. This section presents some results obtained for dynamic pedobarography, using the methods previously described. Other results, for other types of images, are presented in [21, 22, 23].

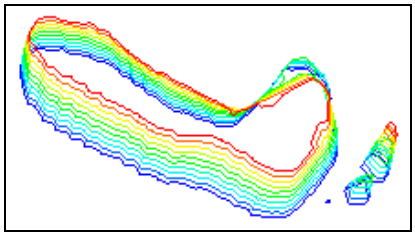

Figure 18. Ten isobaric contours extracted from the surface in Figure 17.

4.1 - Results for Contour Modelling

From the 62-pixel contour shown in Figure 19, a new contour (Figure 20) is built by a rigid geometric transformation consisting of a -15º rotation around the image origin, a -100 pixel translation on the *x*-axis, a -25 pixel translation on the *y*-axis, and a scaling relative to the origin by a factor 1.25.

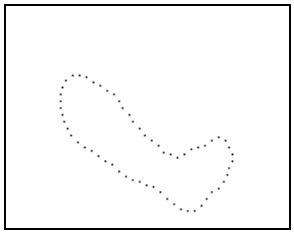

Figure 19. Contour 1.

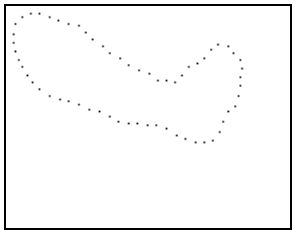

Figure 20. Contour 2.

Using the contour modelling by linear axial finite elements made of rubber, 60 matches were successfully obtained; from those matches the rigid transformation was estimated, using a custom implementation of the unit quaternions method of Horner [24]. The estimated results were: -99.75 for the *x*-axis translation, -24.98 for the *y*-axis translation, a rotation of -14.88º and a scale factor of 1.25. By applying the estimated transformation, except the scaling, to contour 1 and superimposing it on contour 2, the result is as shown in Figure 21, where the matched points are connected for better viewing.

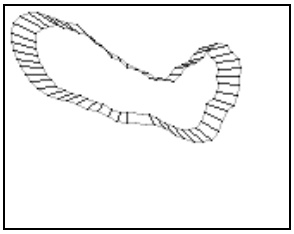

Figure 21. Matches between contours 1 and 2 after the application of the estimated rotation and translation.

Considering now the contours 3 (64-pixel) and 4 (51-pixel) represented in Figures 22 and 23, and using the Sclaroff isoparametric elements made of rubber, 34 successful matches were obtained, as shown in Figure 24. After computing the nodal and modal displacements, the former were applied to contour 3; the result of this transformation is shown in Figure 25. The computed value for the deformation energy was 33.6.

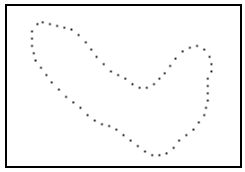

Figure 22. Contour 3.

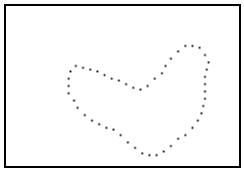

Figure 23. Contour 4.

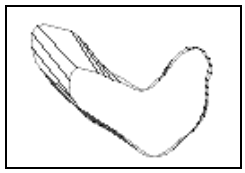

Figure 24. Matches between cntours 3 and 4.

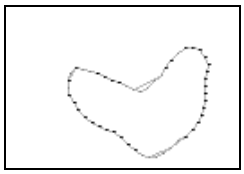

Figure 25. ... after applying the estimated node displacments.

Repeating the process for contours 4 (51-pixel) and 5 (50-pixel) shown in Figures 23 and 26, 33 successful matches are obtained and the computed deformation energy is 6.53; this much lower energy value reflects the fact that these two contours are much more similar than the preceding pair, as shown in Figure 27.

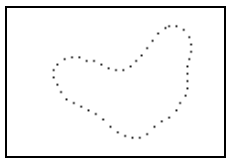

Figure 26. Contour 5.

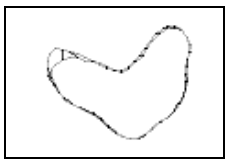

Figure 27. Matches between contours 4 and 5.

4.2. Results for Surface Modelling

Considering now the 127-node in Figure 28 and the 133-node surface in Figure 29, the use of Sclaroff isoparametric elements made of rubber results in 66 successful matches, shown in Figures 30 and 31. The computed deformation energy is 785.97.

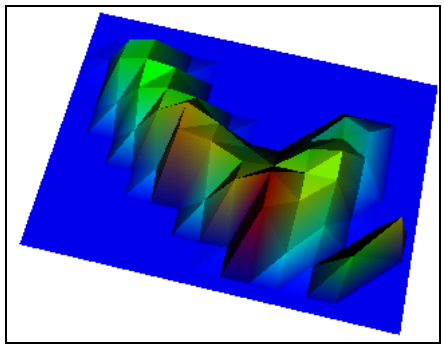

Figure 28. Surface 1.

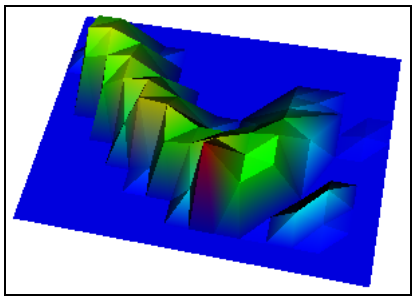

Figure 29. Surface 2.

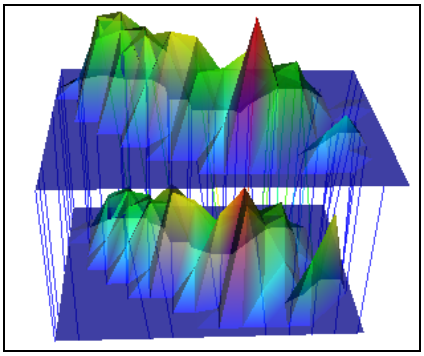

Figure 30. Matches between surfaces 1 and 2.

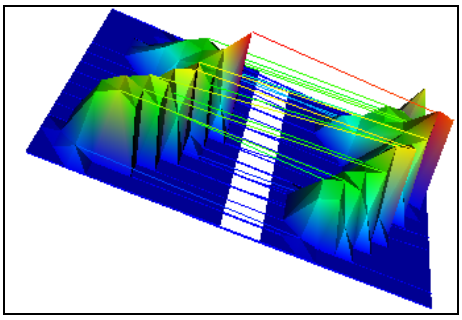

Figure 31. Matches between surfaces 1 and 2 (other view).

Repeating the above process for the 127-node surface in Figure 28 and the 109-node surface in Figure 32, 58 successful matches are obtained, and the resulting deformation energy is 1141.77; the increase in the deformation energy is due to the larger difference between the surfaces, as shown in Figures 33 and 34.

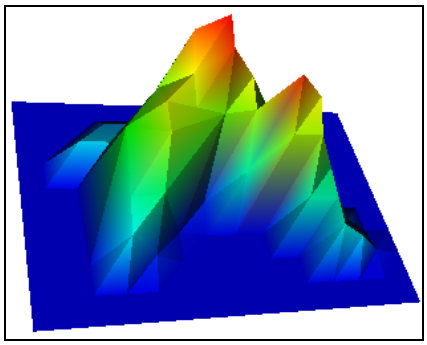

Figure 32. Surface 3.

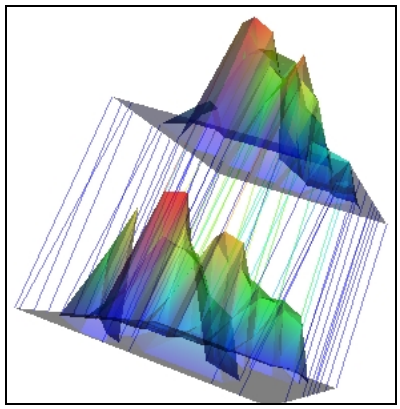

Figure 33. Matches between surfaces 1 and 3.

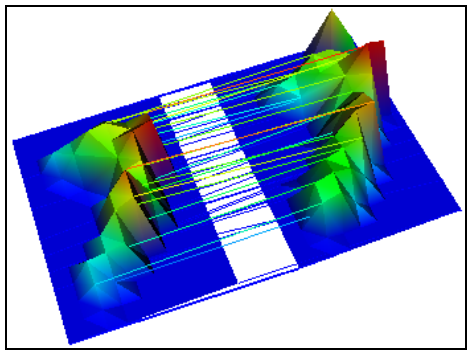

Figure 34 - Matches between surfaces 1 and 3 (other view).

4.3. Results for Isobaric Contour Modelling

Considering the 80-node isobaric contour in Figure 35 and the 70-node isobaric contour in Figure 36, both pertaining to the same surface, and modelling the contours by Sclaroff isoparametric 3D finite elements made of rubber, 43 matches are obtained (Figure 37) and the computed deformation energy is 844.33.

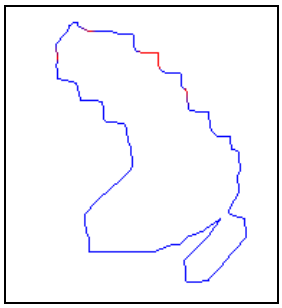

Figure 35. Isobaric contour 1.

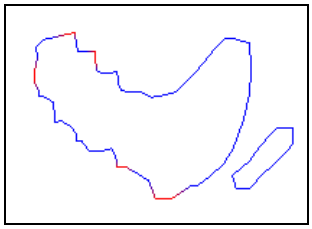

Figure 36. Isobaric contour 2.

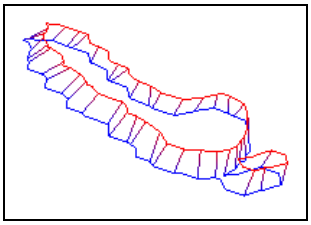

Figure 37. Matches between isobaric contours 1 and 2.

The same process applied to the contour in Figure 35

and the one in Figure 38 (60-node) results in 58 successful matches and in a deformation energy value of 1315.43; again the deformation energy measures correctly the shape dissimilarity, as shown in Figure 39.

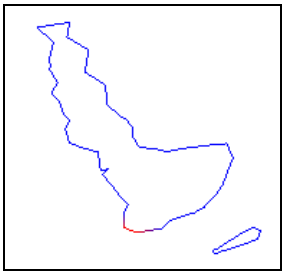

Figure 38. Isobaric contour 3.

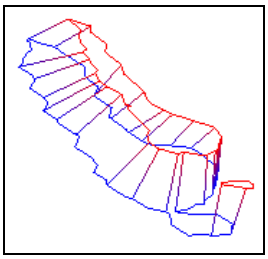

Figure 39. Matches between isobaric contours 1 and 3

5. Conclusion and Further Work

A methodology has been presented for obtaining the correspondence between 2D and 3D objects, rigid or non-rigid, and it has been illustrated for dynamic pedobarography images. The objects are modelled by finite elements and modal analysis is used to define an eigenmode space where the matching is performed. The estimation of the nodal displacement of non-matched nodes is achieved by minimising the deformation energy, through a least squares method, where the material properties of the physical model intervene.

The experimental results shown confirm that satisfactory results are obtained for dynamic pedobarographic image data, both in terms of matching results and in terms of the estimated nodal displacements; the computed deformation energy is also consistent with the subjective similarity between the objects.

In dynamic pedobarography, the use of the pixel brightness values as a third Cartesian co-ordinate is very satisfactory, both in terms of its interpretation as pressure, and in solving the problems associated to merging or the splitting of objects.

Currently, a parallel version of the system is being implemented for a target machine composed by a variable number of heterogeneous networked computers, running under *WPVM - Windows Parallel Virtual Machine*; the preliminary results already obtained are very promising regarding the computational speedup achieved.

Acknowledgement

This work has been done with the support of the PhD grants PRAXIS XXI BD/3243/94 and BD/2850/94 of the first two authors.

References

[1] Stanley Edward Sclaroff, PhD Thesis: *Modal Matching: A Method for Describing, Comparing, and Manipulating Digital Signals*, MIT, 1995

[2] Stan Sclaroff, Alex Pentland, *Modal Matching for Correspondence and Recognition*, IEEE Transactions on Pattern Analysis and Machine Intelligence, Vol. 17, Nº 6, pp. 545-561, June 1995

[3] Alex Pentland, Jonh Williams, *Perception Of Non-Rigid Motion Inference of Shape, Material and Force*, M.I.T. Media Laboratory - Technical Report Nº 113, 1989

[4] S. Graham Kelly, *Fundamentals of Mechanical Vibrations*, McGraw-Hill, 1993

[5] Klaus-Jürgen Bathe, *Finite Element Procedures*, Prentice Hall, 1996

[6] Michael Kass, Andrew Witkin, Demetri Terzopoulos, *Snakes: Active Contour Models*, International Journal of Computer Vision, pp. 321-331, 1988

[7] J. Martin, Alex Pentland, Stan Sclaroff, R. Kikinis, *Characterization of Neuropathological Shape Deformations*, IEEE Transactions on Pattern Analysis and Machine Intelligence, Vol. 20, Nº 3, February 1998

[8] N. H-M. Syn, R. W. Prager, *FEM Eigenmodes as Shape Features*, Cambridge University Engineering Department - Technical Report Nº 211, 1995

[9] N. H-M. Syn, R. W. Prager, *Bayesian Registration of Models using FEM Eigenmodes*, Cambridge University Engineering Department - Technical Report Nº 213, 1995

[10] Alex Pentland, Stan Sclaroff, *Closed-Form Solutions for Physically Based Shape Modeling and Recognition*, IEEE Transactions on Pattern Analysis and Machine Intelligence, Vol. 13, Nº 7, July 1991

[11] Chahab Nastar, PhD Thesis: *Modèles Phisiques Déformables et Modes Vibratoires pour l'Analyse du Mouvement non-rigide dans les Images Multidimensionnelles*, L'École Nationale des Ponts et Chaussées, 1994

[12] A. Jorge Padilha, Luis A. Serra, Susana A. Pires, A. Filipe N. Silva, *Caracterização Espacio-Temporal de Pressões Plantares em Pedobarografia Dinâmica*, FEUP/INEB, 1995

[13] João Manuel R. S. Tavares, Tese de Mestrado: *Obtenção de Estrutura Tridimensional a Partir de Movimento de Câmara*, FEUP, 1995

[14] T. F. Cootes, C. J. Taylor, *Active Shape Model Search using Grey-Level Models: A Quantitative Evaluation*, Proc. British Machine Vision Coference (Ed. J. Illingworth), BMVA Press, pp. 639/648, 1993

[15] T. F. Cootes, C. J. Taylor, *A Unified Approach to Coding and Interpreting Face Images*, Proc.

British Machine Vision Coference (Ed. J. Illingworth), BMVA Press, pp. 639/648, 1993

[16] T. F. Cootes, C. J. Taylor, *Modelling Object Appearence Using The Grey-Level Surface*, Proc. British Machine Vision Coference, pp. 479/488, 1994

[17] Baback Moghaddam, Chahab Nastar, Alex P. Pentland, *Bayesian Face Recognition using Deformable Intensity Surfaces*, MIT Media Laboratory - Technical Report Nº 371, 1996

[18] Will Schroeder, Ken Martin, *The VTK User's Guide*, Kitware Inc., June 1999

[19] Will Schroeder, Ken Martin, Bill Lorensen, *The Visualization Toolkit*, 2nd Edition, Prentice Hall, 1998

[20] Robert Davies, Newmat, *A matrix library in C++*, 1999 - http://webnz.co.nz/robert/

[21] João Manuel R. S. Tavares, J. Barbosa, A. Jorge Padilha, *Determinação da Correspondência entre Objectos, em Visão por Computador, Utilizando o Método dos Elementos Finitos e Análise Modal*, 4º Encontro Nacional do Colégio de Engenharia Electrotécnica, Lisboa, Portugal, 27/28 de Maio de 1999

[22] João Manuel R. S. Tavares, J. Barbosa, A. Jorge Padilha, *Determinação da Correspondência entre Objectos utilizando Modelação Física*, 9º Encontro Português de Computação Gráfica, Marinha Grande, Portugal, 16-18 de Fevereiro de 2000

[23] João Manuel R. S. Tavares, J. Barbosa, A. Jorge Padilha, *Determinação da Correspondência entre Modelos de Contorno e de Superfície, Utilizando Modelização por Elementos Finitos e Análise Modal, em Visão por Computador*, VI Congresso Nacional de Mecânica Aplicada e Computacional, Aveiro, Portugal, 17-19 de Abril de 2000

[24] Berthold K. P. Horn, *Closed-form solution of absolute orientation using unit quaternions*, Journal of the Optical Society of America A, Vol. 4, pp. 629/642, April 1987